Tissue Engineering and Delivery Systems **Biotechnology and Bioengineering**
DOI 10.1002/bit.25572

Application of a Fluorescence Resonance Energy Transfer (FRET)-based Biosensor for Detection of Drug-induced Apoptosis in a 3D Breast Tumor Model†

Padmaja Anand,[1] Afu Fu,[1] Swee H. Teoh,[1] Kathy Q. Luo[1]*

[1]School of Chemical and Biomedical Engineering, Nanyang Technological University, 70 Nanyang Drive, Singapore 637457

KEYWORDS: 3D breast tumor model; fluorescence resonance energy transfer (FRET); biosensor; anti-cancer drugs; real-time detection of apoptosis

* Corresponding author. Address: School of Chemical and Biomedical Engineering, Nanyang Technological University, 70 Nanyang Drive, Singapore 637457. Tel: +65 6790-4257; Fax: +65 6791-1761. E-mail address: kluo@ntu.edu.sg (K.Q. Luo)

† This article has been accepted for publication and undergone full peer review but has-not been through the copyediting, typesetting, pagination and proofreading process, which may lead to differences between this version and the Version of Record. Please cite this article as doi: [10.1002/bit.25572]

Additional Supporting Information may be found in the online version of this article.

Received October 24, 2014; Revision Received February 12, 2015; Accepted February 13, 2015

ABSTRACT

Two-dimensional (2D) cultures are commonly used for testing drug effects largely because of their easy maintenance. But they do not represent the spatial interactions of the cells within a tumor. Three-dimensional (3D) cultures can overcome those limitations thus mimicking the architecture of solid tumor. However, it is not easy to evaluate drug effects in 3D culture for a long time. This necessitates the development of a real-time and longitudinal analysis of 3D platforms. In this study, we transfected the plasmid DNA encoding the fluorescence resonance energy transfer (FRET)-based biosensor into human breast cancer cells and generated two cell lines of MCF7-C3 and MDA-MB-231-C3 (231-C3) cells. We used them to determine the activation of caspase-3, whereby healthy cells appear green and apoptotic cells appear blue by FRET imaging. As the caspase sensors can be constantly produced within the cells and quickly respond to caspase activation, we hypothesized that these sensor cells will allow longitudinal detection of apoptosis. MCF7-C3 and 231-C3 spheroids were generated and subjected to histological examination, gene expression studies, drug treatment and FRET analyses. Our results demonstrated that MCF7-C3 cells formed tight 3D spheroids, and mimicked *in vivo* tumor architecture. The mRNA level of tumorigenic markers such as MMP-9, SOX2 and OCT4A were much higher in cells cultured in 3D than in 2D. Finally, upon treatment with paclitaxel, the FRET effect was reduced at the rim of MCF7-C3 spheroids in a dose and time-dependent manner demonstrating these sensor cells can be used to determine drug-induced apoptosis in a 3D set up. This study supports the possibility of developing a biosensor-based *in vitro* 3D breast tumor model for determination of anti-cancer drug penetration over a long course of time in a non-invasive manner.

Introduction

Globally, breast cancer in women is the leading cause of cancer death with 1,383,500 estimated new cases each year (Jemal et al., 2011). This has generated an interest to obtain insights on breast tumorigenesis and also to develop drugs that effectively combat the disease. Conventionally, petri dish cultures and small animal models have been used to evaluate the efficacy of drug treatment and to determine the factors responsible for tumor progression. However, these two-dimensional (2D) monolayers differ from *in vivo* tumors in their cell-cell and cell-extracellular matrix (ECM) interactions, and are therefore unsuitable platforms for understanding *in vivo* tumor responses. Additionally, the malignancy and the signaling pathways are masked in such cultures (Green and Yamada, 2007; Pickl and Ries, 2008; Yamada and Cukierman, 2007). Owing to the lack of suitable *in vitro* platforms, animal models are the primary choice for conducting cancer research, even though they have differences in terms of physiology and microenvironment, and high cost (Kelland, 2004; Teicher, 2006). More importantly, not every type of human cancer cells can form solid tumors in nude mice. Therefore, there is an urgent need to develop three-dimensional (3D) *in vitro* models which better recapitulate breast tumor for drug efficacy and mechanism studies.

Currently, multicellular tumor spheroids are well-established and accepted as advanced tools for cancer drug screening. In this respect, many techniques are available to generate such spheroids: hanging drop (Ramsey, 2011), microcarrier beads (Jessup et al., 1997), and rotary cultures (Zheng et al., 2012). However, these methods have limitations which can be overcome by the non-adhesive coating technique enabling the formation of spheroids in uniform size. Moreover, this method is straightforward, does not use any chemicals, and is reproducible (Ivascu and Kubbies, 2006). Recently, Guo et al., developed a magnetic 3D spheroid platform by using non-adhesive plates (Guo et al., 2014).

Along with the establishment of *in vitro* 3D tumor models, techniques of evaluating cellular responses to drugs were developed. Current techniques include dissociating the spheroids for manual counting or cell viability assessments using commercial reagents (Ho et al., 2012), by quantification using flow cytometry (Woods et al., 1996), or by immunostaining techniques (Bressenot et al., 2009). Despite their accuracy, these assays do not allow real-time monitoring and longitudinal follow-up. On this note, a potential solution may be live-cell imaging using biosensors that provide sensitive, rapid and non-invasive readouts for drug-induced effects in different microenvironments. FRET has been extensively used to map protein interactions by distant-dependent energy transfer from donor chromophore to acceptor chromophore. It is highly sensitive and robust. Our group has previously established the use of FRET for monitoring the activation of caspase-3 enzyme (Luo et al., 2001), which can be activated by both intrinsic and extrinsic pathways in apoptosis. Previously, our group has applied this FRET-based caspase-3 (C3) biosensor in HeLa cells to assess a potent anti-cancer compound from herbal plant (Tian et al., 2007). The C3 biosensor consists of three parts: a cyan fluorescent protein (CFP), a protein linker (amino acid sequence Asp-Glu-Val-Asp (DEVD), corresponding to the cleavage site of caspase 3) and a yellow fluorescent protein (YFP). On excitation of the donor CFP of live cells, efficient energy transfer takes place to the acceptor YFP, resulting in green fluorescence of the cells. However, when the cells undergo apoptosis, the caspase cascade is activated. Caspase-3 then cleaves the protein linker (DEVD) between the fluorescent proteins and eliminates the energy transfer. This results in the blue fluorescence of the cells. Therefore, the C3 sensor allows us to monitor the dynamics of caspase-3 during apoptosis in live cells.

In this study, we have analysed different 3D culturing methods and established that multicellular tumor spheroids obtained with non-adhesive coating technique provided high

reproducibility, better handling and is physiologically representative of *in vivo* tumors. In addition, we have applied this FRET-based biosensor for obtaining *in situ* assessments on microenvironment-based drug effects on live cells. The breast tumor spheroids, in combination with the sensitive and specific C3 biosensor, provide a proof-of-concept of live-cell imaging in three dimensions.

Materials and Methods

Cell Culture

The plasmid DNA for C3 biosensor, containing the CFP-DEVD-YFP fusion gene, was generated and characterized by our group previously (Luo et al., 2001). The breast cancer cell lines, MCF-7 and MDA-MB-231, were purchased from ATCC and later transfected with this C3 biosensor plasmid to generate two stable cell lines designated as MCF7-C3 and 231-C3 respectively in this study. These cells were cultured in Dulbecco's modified Eagle's medium – high glucose (Gibco, USA) supplemented with 10% fetal bovine serum (Hyclone, USA) and 100 units per mL penicillin plus 100 mg/mL streptomycin (Gibco, USA). The cells were incubated at 37°C with an atmosphere maintained at 5% CO_2.

Generation of Multicellular Tumor Spheroids (MCTS)

Microencapsulation

2% (w/v) alginate solution and 2% (w/v) gelatin was mixed at 1:1 ratio thoroughly and then mixed with 1,000,000 cells/mL of MCF7-C3 cells. To generate the beads, droplets of cell suspension in ECM-mimicking alginate-gelatin mixture was slowly extruded into 100 mmol/L $CaCl_2$ using a 30-gauge needle. The beads were allowed to gel completely for 5 min before incubating them in their complete growth media (DMEM + 20% FBS and 1% penicillin-streptomycin). The average size of the beads ranged from 2,400 -2,600 μm and about 10,000 cells were encapsulated in each bead (Figure 1A).

Hanging Drop Method

MCF7-C3 cells grown on tissue culture flasks were trypsinized using 0.25% trypsin-EDTA (Gibco, USA) to obtain single cell suspension. Then, the spheroids were generated as described

previously (Kurosawa, 2007). Briefly, 30 µL of cell suspension was dropped onto the lid of a 100 mm diameter petri dish. 30 droplets were placed per petri dish to prevent any coalescence. The lid was placed on the petri dish containing 10 mL PBS to ensure hydration. The spheroids were generated after 2 days incubation at 37°C and 5% CO_2 (Figure 1B).

Non-adhesive Coating

Low adherent round–bottom 96 well plates were employed to generate spheroids. The non-adhesive coating was generated by using 1% Pluronic F-127 (Sigma, USA). The cell suspension is diluted to obtain 5,000 cells in 200 µL of medium. The plate was then centrifuged at 1,000g for 5 min (Ivascu and Kubbies, 2006). Twenty-four hours incubation at 5% CO_2 and 37°C was provided to complete the compaction of single cells to spheroids (Figure 1C).

Drug Treatment

For 2D monolayer, 10,000 MCF7-C3 cells were seeded on a 96 well plate and incubated overnight. For 3D culture, spheroids using 5,000 cells in 200 µl media were generated as described before. Then, paclitaxel, a chemotherapeutic agent, was added into growth media at the concentrations of 20, 200 and 2000 nmol/L. The duration of drug treatment was 72 h. For both culturing methods, untreated controls were cultured in parallel.

Detection of Apoptosis using FRET Imaging Microscopy

MCF7-C3 cells, cultured in monolayers and spheroids, were subjected to different concentrations of paclitaxel to examine the responses to drug treatment based on different culturing methods. After treatment with paclitaxel, fluorescent images were obtained using an inverted fluorescence microscope (Zeiss Axiovert 100, Germany). The cells were excited at 436 ± 10 nm. The

corresponding YFP and CFP images were obtained using 535 ± 15 nm and 480 ± 20 nm filters and recorded using a SPOT CCD camera (Diagnostic Instruments, USA).

Image-based Analysis of FRET Emission Ratio

The images were quantified using ImageJ software. Briefly, the spheroids were partitioned as center (80%) and rim (20%) of the spheroids and their corresponding YFP and CFP images were quantified individually for their fluorescence intensities. A region of interest (ROI) was marked in these assigned portions of the spheroids (center and rim) and the Y/C emission ratio was obtained by using the following formula: FRET emission ratio = $(YFP_{spheroid} - YFP_{background}) / (CFP_{spheroid} - CFP_{background})$ (Tian et al., 2007). The plot profile for the individual YFP and CFP channels were also obtained for the control and drug-treated spheroids using the software.

***In vivo* MCF-7 Tumor Model**

All experiments on animals were conducted in accordance to and approved by the Institutional Animal Care and Use Committee (IACUC) of Nanyang Technological University (NTU). One oestrogen pellet (50 mg/pellet, Innovative Research of America, USA) was implanted subcutaneously to an eight-week-old female BALB/c nude mouse. Four days later, 1 million of MCF-7 cells suspended in 100 μL Matrigel (BD Biosciences, USA) were subcutaneously injected into the mammary fat pad of nude mouse (purchased form BioLasco Company, Taiwan). Eight weeks later, the xenograft tumors were removed from the animal and the tumor tissues were immediately frozen in the liquid nitrogen and then stored at -80°C. The tumors were later subjected to H&E staining.

Sample Fixation, Paraffin Embedding and Hematoxylin and Eosin Staining

The spheroids after five days of culture were fixed with 4% paraformaldehyde at 4°C for overnight. The fixed samples were processed and embedded in paraffin wax. The paraffin blocks were sectioned at 3 µm thicknesses using a rotary microtome and collected in a clean Polysine® slides (Thermo Scientific, USA). For the xenograft tumor, the samples were fixed in Leica OCT Cryocompound tissue-freezing medium (Leica Microsystems, Germany) and cryosectioned at 5 µm thickness using a cryostat and collected in a clean Polysine® slides (Thermo Scientific, USA). Subsequently, sectioned samples were stained with haematoxylin and eosin (H&E) staining and mounted with a coverslip using mounting media.

Gene Expression Analysis

Gene expression analysis was carried out using quantitative real-time polymerase chain reaction (RT-qPCR) which was used in our previous study (Yu et al., 2014). Briefly, total mRNA was collected using TRIzol reagent (Life Technologies, USA) after dissociating the spheroids using StemPro® Accutase® (Life Technologies, USA). The total mRNA was purified using RNeasy Plus Mini Kit (Qiagen, Valencia, CA) and subsequently reverse-transcribed to cDNA. Afterwards, qPCR was carried out using iQ SYBR green supermix and iQ qPCR system (Bio-Rad, USA). For quantification, gene expression relative to the house-keeping gene, GAPDH, was calculated and represented using the comparative method, $2^{-\Delta\Delta CT}$. Table 1 lists the primer sets used in this experiment (AIT Biotech, Singapore). All the reagents necessary for reverse transcription and qPCR was purchased from Promega, USA and Bio-Rad, USA, respectively. All the qPCR reactions were conducted in triplicates.

Statistical Analysis

All the experiments were performed independently for three times and data was presented as mean ± SD. Statistical significance were determined using student t-test or linear regression test as applicable and $^{*}p < 0.05$, $^{**}p < 0.01$ and $^{***}p < 0.001$ were used to indicate the levels of statistical significance.

Results

Comparison of 3D Culture Models for the Generation of Spheroids

To establish a three-dimensional system that closely mimics the *in vivo* situation of tumors, we have compared three different methods to culture cells in 3D for their robustness and suitability for drug testing. Although microencapsulation resulted in the formation of microcapsules with prolonged viability, cellular attachment was lacking. Even when seeding densities higher than the other two methods were used, spheroidal growth was not observed (Figure 1A). The hanging drop method formed irregular spheroids after 2 days. In addition, difficulty in medium exchange posed a problem in maintenance of these spheroids for long-term studies (Figure 1B). Using a cell suspension combined with centrifugation, we generated spheroids in 24 h with uniformed size and in large quantity (Figure 1C). Since the advantages of the third method can support the use of spheroids in high throughput drug screening, we chose this non-adhesive coating technique over the other two approaches in the subsequent experiments.

FRET–based MCF7-C3 Cells Demonstrated Real-Time Live/Dead Read-Outs in both 2D and 3D Cultures

To visualize cell apoptosis in real-time, we took the advantage of the C3 sensor which was shown to be responsive to various apoptotic inducers including UV-light and anticancer drugs (Luo et al., 2001; Tian et al., 2007). The principle of which is clearly illustrated in Figure 2A. As shown in Figure 2B, MCF7-C3 cells seeded directly on petri dishes proliferated and formed monolayers. On the other hand, suspended cells formed spheroids with tight cell contacts. 2D cultures validated the real-time observation of apoptotic cells (blue fluorescence) and live cells (green fluorescence) (Figure 2B and C). Importantly, the 3D spheroids also allowed for the visualization of live cells (green fluorescence). The application of this sensor in our study is

suitable as many chemotherapeutic drugs activate apoptotic cascades in neoplastic cells (Johnstone et al., 2002).

Spheroid Diameter of MCF7-C3 and 231-C3 Cells Dependent on Initial Seeding Density

Different concentrations of cells ranged from 2,500 to 10,000 were used to form the spheroids. A strong correlation between the number of cells and the size of spheroids (n = 5 spheroids) was observed for both MCF7-C3 (R^2 = 0.994) and 231-C3 cells (R^2 = 0.935) (Figure 3B). The size of 231-C3 spheroids (ranging from 575 to 1,023 µm) was two times larger than the diameter of MCF7-C3 spheroids (ranging from 349 to 560 µm) (Figure 3B). However, 231-C3 cells formed looser aggregates, whereas MCF7-C3 cells formed tighter spheroids which should be similar to the compact cellular structure in a tumor. Henceforth, MCF7-C3 cells were used for further evaluation.

Development of Necrotic Core in Spheroidal Cultures

The inefficient transfer of nutrients and wastes beyond 150-200 µm through cellular barrier results in low oxygen centers, leading to nuclear fragmentation and necrosis within the spheroid. This was visualized by H&E staining of a spheroid which was generated by seeding 10,000 MCF7-C3 cells and cultured for 5 days (Figure 4). The absence of the hematoxylin staining of the nuclei in the core of spheroid indicated the presence of necrotic cells in the central region. Furthermore, the presence of hematoxylin staining in the peripheral region of the spheroid (~ 200 µm) suggests the presence of nuclei in these cells. Additionally, the morphological features and the necrotic core observed in the histological sections of the xenograft tumors further demonstrated that the spheroids were able to represent the histological state of tumors *in vivo.* It

can also be observed that from both conditions, the cells at the periphery are more closely packed than the cells located between the necrotic core and periphery.

Up-regulation of Tumorigenic Markers in Spheroids

Overexpression of certain biomarkers such as matrix metalloproteases (MMPs) mediates tumor metastasis *in vivo.* MMPs are essential in degrading ECM to facilitate invasion and metastasis and is highly expressed in metastatic breast tumors (Incorvaia et al., 2007). Real-time qPCR analysis revealed that the transcriptions of MMP-9 in MCF7-C3 spheroids were significantly increased by 1.89 ± 0.73-fold relative to the same cells in monolayers (Figure 5). It has been reported previously that elevated expression of SRY-related HMG box protein (SOX2) and POU domain class 5 transcription factor 1 (OCT4A) were representative of an acquired malignant phenotype in a breast cancer *in vitro* model (Chen et al., 2012). Similarly, tumorigenic markers of SOX2 and OCT4A were upregulated by 6.25 ± 1.36 and 2.30 ± 0.54 fold respectively in MCF7-C3 spheroids (Figure 5), thereby demonstrating that 3D spheroids are a better *in vitro* model than 2D monolayer in revealing the expression of tumorigenic markers.

Differential Response of MCF7-C3 Cells to Paclitaxel in 2D and 3D

In order to compare the drug response between 2D and 3D, high concentration (2000 nmol/L) of paclitaxel was added to the MCF7-C3 cells for 72 h. As expected, 2D monolayer cultures displayed high percentage of cell death (70%) to high dose of paclitaxel, which was determined by analysing the FRET images of over 400 cells. In contrast, 3D spheroids showed different results, with the cells in the rim region displayed blue color indicating the cells died of apoptosis, while most of the cells in the central region appeared green in color indicating those cells were resistant to drug treatment (Figure 6A and Supplementary Figure 1). This was further

substantiated by measuring the fluorescence intensity of MCF7-C3 spheroids under YFP and CFP channels using the plot profile function in ImageJ software (Figure 6B). It can be observed that in the central region of both control and drug-treated spheroids, the emission intensity of YFP is much higher than the intensity of CFP which resulted in a high emission ratio of YFP/CFP (1.99 – 2.20). Interestingly, at the rim region of the drug treated group, the intensity of CFP was elevated which resulted in a reduction of the YFP/CFP emission ratio to 0.90 – 0.91. As the emission ratio of YFP/CFP can be used to represent the FRET effect, this result indicated that these sensor cells can detect apoptosis in a 3D set up. More importantly, in comparison to the 2D monolayer culture, the application of these sensor cells in 3D allowed us to evaluate the spatial response of the cells to the drug treatment.

***In Situ* Assessment of Paclitaxel-induced Apoptosis in MCF7-C3 Spheroids**

Since FRET-based C3 sensor enables real-time and non-invasive detection of apoptosis, longitudinal studies of spheroid integrity with and without drug treatment were conducted. From Figure 7, it was observed that after 48 h of paclitaxel treatment, the onset of apoptosis was visualized. After 72 h, the dose-dependent effect of the drug on the spheroids was observed, with more apoptotic cells appeared in the rim region when the drug concentrations were increased. But more live cells appeared in the central region as evident by the strong green fluorescence in those cells (Supplementary Figure 2). This was further substantiated by measuring the FRET effects at different regions of the spheroids such as the rim and the center (Figure 7B and C). It can be observed from Figure 7B that the FRET effect was reduced by 47% between the control and 2,000 nmol/L of paclitaxel at 72 h. However, much less FRET reduction (25%) was detected between the same two groups at the same time (Figure 7C). Taken together, these results indicate

that these sensor cells-based 3D models can be used to detect the apoptotic effect of anti-cancer drugs in situ and in real-time.

Discussion

Three-dimensional *in vitro* cell culture has been extensively employed in advancing our knowledge on tumorigenesis and also as a platform to test different treatment modalities. This can be attributed to the better tumor biomimetic ability of these 3D models with respect to 2D (Yamada and Cukierman, 2007).

On this note, majority of the available 3D models have been able to recapitulate tumor architecture that is analogous to biological tumors, where a proliferating rim is supported by a necrotic core due to the lack of oxygen and nutrient diffusion. In our results, we have demonstrated a similar tumor architecture (Figure 4), that was previously illustrated by Brahimi-Horn et al (Brahimi-Horn et al., 2007). This technique of generating spheroids has been shown to be reproducible, and is advantageous to other methods such as microencapsulation (Figure 1). Through the formation of tight spheroids with intimate cell-cell interactions, ECM laydown may be similar to physiological conditions, which may be substantiated by the necrotic core.

In this study, we observed the upregulation of SOX2 and OCT4A and MMP-9, key proteins in ECM degradation which further facilitate tumor metastasis. The physiologically relevant architecture and hypoxic core in the spheroids lead to the modulation of genes associated with metastasis and tumorigenesis (Su et al., 2013). A similar expression pattern has been reported by Chen Lei et al., using breast tumor cells cultured on 3D collagen scaffolds, suggesting the enhanced tumor stem cell properties in 3D (Chen et al., 2012). Together, this demonstrated that 3D cultures are more physiologically relevant as compared to their 2D counterparts in their

morphology, multi-layered arrangement and gene expression, making it a superior platform to study *in vivo*-like responses to drug candidates.

Evaluation of cell fate on drug treatment is carried out using methods ranging from histology (Bressenot et al., 2009) to biochemical assays (Ho et al., 2012) which are inherently destructive and time-consuming. In addition, real-time dynamics of microenvironment-dependent effects of drug treatment cannot be obtained. Real-time assessments provide precise tracking of treatment response and provide biologically relevant understanding of tumor progression and/or mechanism of drug action. In this regard, FRET-based biosensors can provide high-resolution real-time monitoring of protein interactions in cells (Chirico, 2009). In addition, chemotherapeutic drugs are known to kill tumor cells by activating apoptotic signaling pathways (Hannun, 1997). Therefore, by utilizing the C3 biosensor, a rapid and sensitive evaluation of apoptosis can provide ample information on chemotherapy-induced cell death and apoptosis (Luo et al., 2001; Tian et al., 2007; Zhu et al., 2012). This study proved the feasibility of FRET in assessing longitudinal analysis of the drug-induced effects in a real-time and non-invasive manner, without any post-processing requirements in three dimensions.

Our results clearly demonstrated that spheroids were more resistant to drug treatment than monolayers, which correlated with similar observations with other drugs (Pickl and Ries, 2008; Yip and Cho, 2013). This resistance can be due to the poor penetration within the spheroids, and/or mechanism of action of paclitaxel on proliferating cells rather than quiescent cells (Nicholson et al., 1997). Another factor would be heterogeneity in the spheroids which make some cells intrinsically drug resistant and fail to activate apoptotic machinery (Hannun, 1997). Further studies may be required to understand if combinational therapy may provide synergistic effects in eliminating this drug resistance.

Conclusion

This study was aimed at developing a novel platform for real-time and non-invasive imaging of three-dimensional spheroids using FRET imaging. Our results have demonstrated that FRET-based biosensor may be useful for obtaining *in situ* information of apoptotic effects induced by drug candidates in 3D biomimetic system. The results obtained by using common endpoint assays such as histology and gene expression, plus cell imaging analysis showed that spheroids generated using the non-adhesive coating plus centrifugation method were more physiological than 2D cultures. Taken together, these results show the potential of these FRET sensor-based 3D spheroids serving as an *in vitro* tumor model for longitudinal monitoring of drug-induced apoptotic effects.

Acknowledgements

This work was supported by the National Research Foundation of Singapore (NRF-CRP grant: M4092018.0S4) and Ministry of Education (AcRF-Tier 1 grant: M4011279.120 RG35/14). The authors declare no conflict of interest.

References

Brahimi-Horn MC, Chiche J, Pouysségur J. 2007. Hypoxia and cancer. Journal of molecular medicine 85(12):1301-1307.

Bressenot A, Marchal S, Bezdetnaya L, Garrier J, Guillemin F, Plénat F. 2009. Assessment of apoptosis by immunohistochemistry to active caspase-3, active caspase-7, or cleaved PARP in monolayer cells and spheroid and subcutaneous xenografts of human carcinoma. Journal of Histochemistry & Cytochemistry 57(4):289-300.

Chen L, Xiao Z, Meng Y, Zhao Y, Han J, Su G, Chen B, Dai J. 2012. The enhancement of cancer stem cell properties of MCF-7 cells in 3D collagen scaffolds for modeling of cancer and anti-cancer drugs. Biomaterials 33(5):1437-1444.

Chirico G. 2009. Bioimaging: Protein watching. Nature Photonics 3(2):81-82.

Green JA, Yamada KM. 2007. Three-dimensional microenvironments modulate fibroblast signaling responses. Advanced drug delivery reviews 59(13):1293-1298.

Guo WM, Loh XJ, Tan EY, Loo SCJ, Ho VH. 2014. Development of a magnetic 3D spheroid platform with potential application for high-throughput drug screening. Molecular pharmaceutics.

Hannun YA. 1997. Apoptosis and the dilemma of cancer chemotherapy. Blood 89(6):1845-1853.

Ho WY, Yeap SK, Ho CL, Rahim RA, Alitheen NB. 2012. Development of multicellular tumor spheroid (MCTS) culture from breast cancer cell and a high throughput screening method using the MTT assay. PLoS One 7(9):e44640.

Incorvaia L, Badalamenti G, Rini G, Arcara C, Fricano S, Sferrazza C, Di Trapani D, Gebbia N, Leto G. 2007. MMP-2, MMP-9 and activin A blood levels in patients with breast cancer or prostate cancer metastatic to the bone. Anticancer research 27(3B):1519-1525.

Ivascu A, Kubbies M. 2006. Rapid generation of single-tumor spheroids for high-throughput cell function and toxicity analysis. Journal of Biomolecular Screening 11(8):922-932.

Jemal A, Bray F, Center MM, Ferlay J, Ward E, Forman D. 2011. Global cancer statistics. CA: a cancer journal for clinicians 61(2):69-90.

Jessup JM, Brown D, Fitzgerald W, Ford R, Nachman A, Goodwin T, Spaulding G. 1997. Induction of carcinoembryonic antigen expression in a three-dimensional culture system. In Vitro Cellular & Developmental Biology-Animal 33(5):352-357.

Johnstone RW, Ruefli AA, Lowe SW. 2002. Apoptosis: a link between cancer genetics and chemotherapy. Cell 108(2):153-164.

Kelland L. 2004. "Of mice and men": values and liabilities of the athymic nude mouse model in anticancer drug development. European Journal of Cancer 40(6):827-836.

Kurosawa H. 2007. Methods for inducing embryoid body formation: *In vitro* differentiation system of embryonic stem cells. Journal of bioscience and bioengineering 103(5):389-398.

Luo KQ, Yu VC, Pu Y, Chang DC. 2001. Application of the fluorescence resonance energy transfer method for studying the dynamics of caspase-3 activation during UV-induced apoptosis in living HeLa cells. Biochemical and biophysical research communications 283(5):1054-1060.

Maity G, Choudhury PR, Sen T, Ganguly KK, Sil H, Chatterjee A. 2011. Culture of human breast cancer cell line (MDA-MB-231) on fibronectin-coated surface induces pro-matrix metalloproteinase-9 expression and activity. Tumor Biology 32(1):129-138.

Nicholson K, Bibby M, Phillips R. 1997. Influence of drug exposure parameters on the activity of paclitaxel in multicellular spheroids. European Journal of Cancer 33(8):1291-1298.

Pickl M, Ries C. 2008. Comparison of 3D and 2D tumor models reveals enhanced HER2 activation in 3D associated with an increased response to trastuzumab. Oncogene 28(3):461-468.

Ramsey F. 2011. A simple hanging drop cell culture protocol for generation of 3D spheroids. Journal of Visualized Experiments(51).

Su G, Zhao Y, Wei J, Han J, Chen L, Xiao Z, Chen B, Dai J. 2013. The effect of forced growth of cells into 3D spheres using low attachment surfaces on the acquisition of stemness properties. Biomaterials 34(13):3215-3222.

Teicher BA. 2006. Tumor models for efficacy determination. Molecular cancer therapeutics 5(10):2435-2443.

Tian H, Ip L, Luo H, Chang D, Luo K. 2007. A high throughput drug screen based on fluorescence resonance energy transfer (FRET) for anticancer activity of compounds from herbal medicine. British journal of pharmacology 150(3):321-334.

Woods ML, Koch CJ, Lord EM. 1996. Detection of individual hypoxic cells in multicellular spheroids by flow cytometry using the 2-nitroimidazole, EF5, and monoclonal antibodies. International Journal of Radiation Oncology* Biology* Physics 34(1):93-101.

Yamada KM, Cukierman E. 2007. Modeling tissue morphogenesis and cancer in 3D. Cell 130(4):601-610.

Yip D, Cho CH. 2013. A multicellular 3D heterospheroid model of liver tumor and stromal cells in collagen gel for anti-cancer drug testing. Biochemical and biophysical research communications 433(3):327-332.

Yu T, Zhou Z, Mu Y, de Lima Lopes G, Luo KQ. 2014. A novel anti-cancer agent, acetyltanshinone IIA, inhibits oestrogen receptor positive breast cancer cell growth by down-regulating the oestrogen receptor. Cancer letters 346(1):94-103.

Zheng H, Tian W, Yan H, Yue L, Zhang Y, Han F, Chen X, Li Y. 2012. Rotary culture promotes the proliferation of MCF-7 cells encapsulated in three-dimensional collagen–alginate hydrogels via activation of the ERK1/2-MAPK pathway. Biomedical Materials 7(1):015003.

Zhu X, Fu A, Luo KQ. 2012. A high-throughput fluorescence resonance energy transfer (FRET)-based endothelial cell apoptosis assay and its application for screening vascular disrupting agents. Biochemical and biophysical research communications 418(4):641-646.

Figure Legends

Figure 1. Comparison between 3D cell culture methods. (A) Microencapsulation of 10,000 MCF7-C3 cells in alginate-gelatin mixture (1:1). (B) Hanging drop method using 5,000 cells to obtain spheroids after two days of incubation. (C) Non-adhesive coating of 96 round-bottom well plates to generate MCF7-C3 spheroids of 5,000 cells. Scale bar: 100 μm.

Figure 2. (A) Principle of FRET biosensor. (B and C) Morphological variation of MCF7-C3 cells when grown as a confluent monolayer and as a 3D tumor spheroid using non-adhesive coating method. The YFP and CFP images were individually taken and then overlaid to obtain the merged FRET image. Scale bar: 100 μm. (C) Enlarged fluorescent images of MCF7-C3 cells under YFP and CFP channels from 2D and also the merged FRET image from 2D and 3D, where live cells appeared in green (yellow arrow) and apoptotic cells appeared in blue (red arrow). Scale bar 50 μm.

Figure 3. Formation of spheroids of varying initial seeding densities on non-adhesive coated plates. (A) 2,500, 5,000, 7,500 and 10,000 cells of MCF7-C3 or 231-C3 were seeded in round-bottom well plates and observed after 24 h to determine the correlations between seeding density and size of spheroids in these two cell lines (YFP images). Scale bar 100 μm. (B) Diameter of each spheroid was measured using ImagePro Plus software. The mean diameter averaged from 15 spheroids generated from three independent experiments was plotted against cell seeding density to determine the R^2 value in a linear regression curve.

Figure 4. Hematoxylin and eosin staining of MCF7-C3 spheroids and xenograft tumor of MCF-7 cells. Enlarged images of the spheroid and xenograft tumor from the boxed regions. Scale bar: 50 μm.

Figure 5. Relative expression of tumorigenic markers between 2D and 3D. Expression levels of MMP-9, SOX2, and OCT4A were compared between MCF7-C3 cells in 3D spheroids and 2D monolayers by qRT-PCR. Results are shown as mean ± s.d. GAPDH was employed as an internal control.

Figure 6. Apoptotic effects of paclitaxel. (A) 10,000 MCF7-C3 cells seeded in 96-well plate (2D) were treated with high concentration (2000 nmol/L) of paclitaxel and observed after 72 h incubation. Similar treatment conditions were applied to spheroids of 5,000 MCF7-C3 cells. Scale bar 100 µm. (B) The intensity of YFP and CFP across the spheroid was measured separately using the plot profile function in the ImageJ software. The yellow line represents the profile along which the measurement was made. Rim region counts for 20%, while the center accounts for the 80% of the spheroid.

Figure 7. *In situ* visualization of spheroids. (A) Effects of drug treatment at different concentrations of paclitaxel on spheroid integrity captured spatially and temporally without disrupting the spheroid. The yellow arrow points to the intact circumference of the control spheroid whereas the red arrow points to the apoptotic mass at the rim of the drug-treated spheroid at 72 h. Scale bar 100 µm. (B) Relative YFP/CFP emission ratio quantification for different paclitaxel concentrations over time at the rim of the spheroid. (C) Relative YFP/CFP emission ratio at the center of the spheroid.

Supplementary Figure 1. Fluorescent images of MCF7-C3 cells under YFP and CFP channels and also the merged FRET image from 3D, where live cells appeared in green and apoptotic cells appeared in blue. Scale bar 100 µm.

Supplementary Figure 2. Fluorescent images of MCF7-C3 spheroids at 72 h under YFP, CFP channels and the merged FRET image when treated with different concentrations of paclitaxel. The live cells appeared in green and apoptotic cells appeared in blue. Scale bar 100 μm.

Table 1. qPCR forward and reverse primer sequences for tumorigenic and internal markers.

Gene	Accession number/ reference	Primer sequence (5'→ 3')
MMP-9	NG_011468	F: GGGCTTAGATCATTCCTCAGTG
		R: GCCATTCACGTCGTCCTTAT
SOX2	(Chen et al., 2012)	F: CCCCTTTATTTTCCGTAGTTGTATTT
		R: GATTCTCGGCAGACTGATTCAA
OCT4A	(Chen et al., 2012)	F: CCCCTGGTGCCGTGAAG
		R: GCAAATTGCTCGAGTTCTTTCTG
GAPDH	(Maity et al., 2011)	F: CGGAGTCAACGGATTTGGTCGTAT
		R: AGCCTTCTCCATGGTGGTGAAGAC

Figure 1

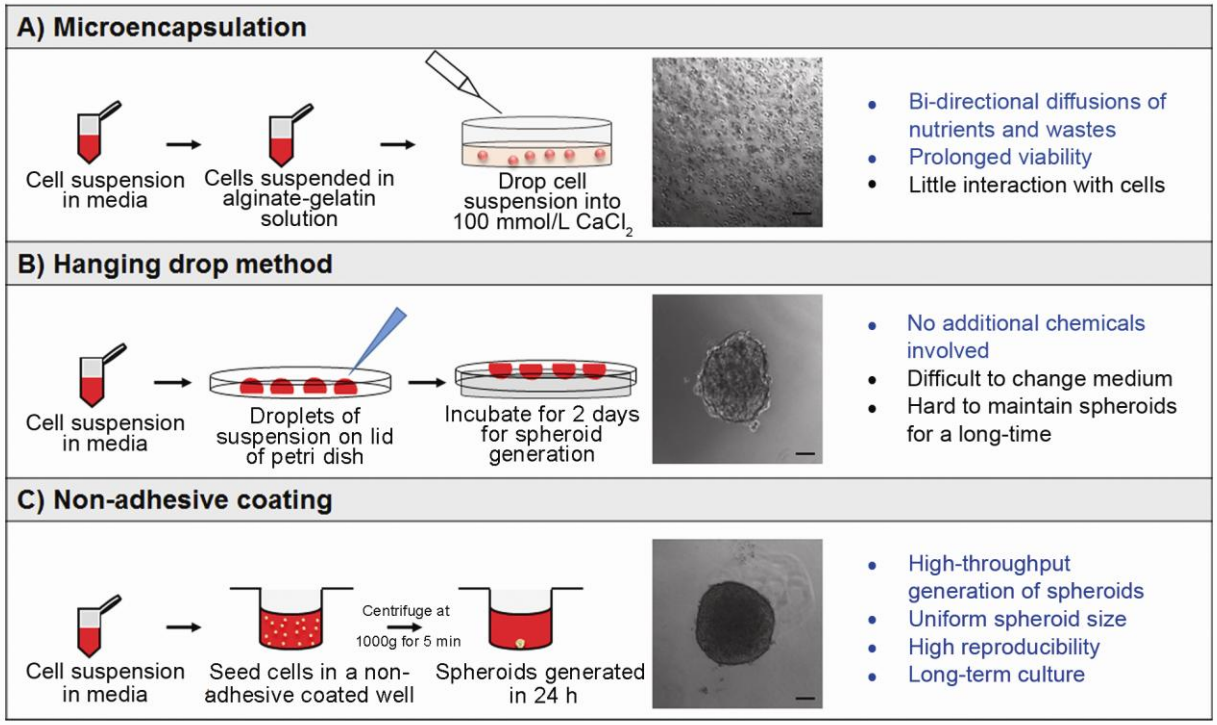

Figure 2

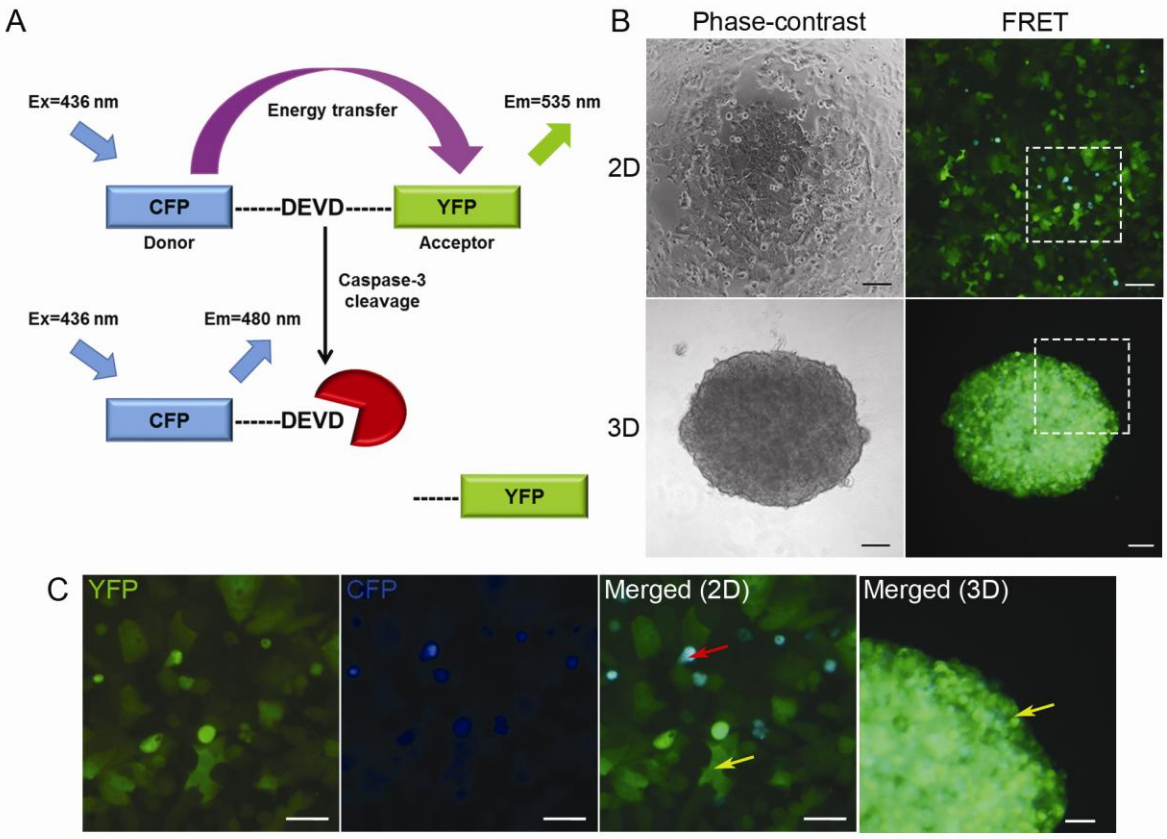

Figure 3

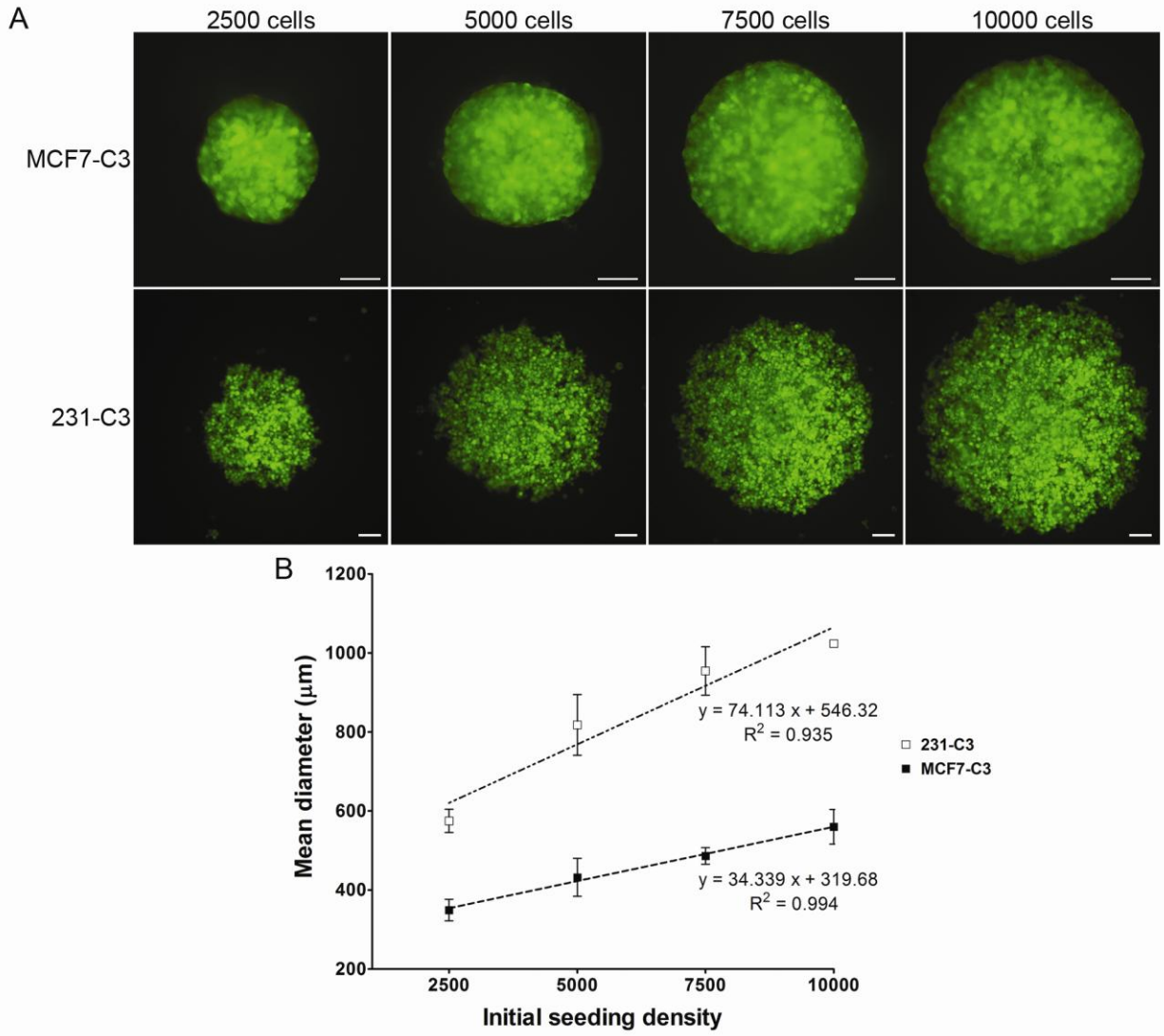

Figure 4

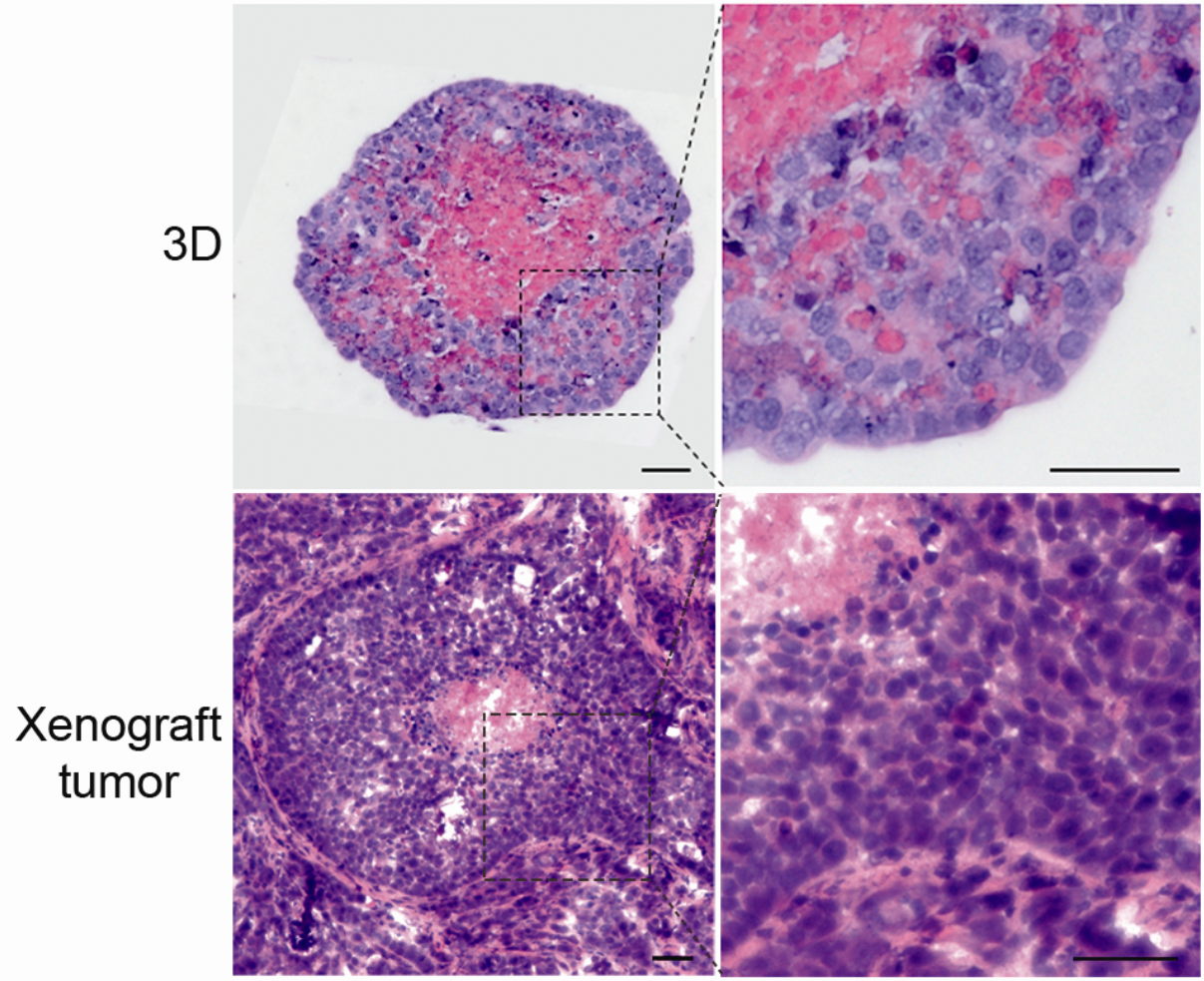

Figure 5

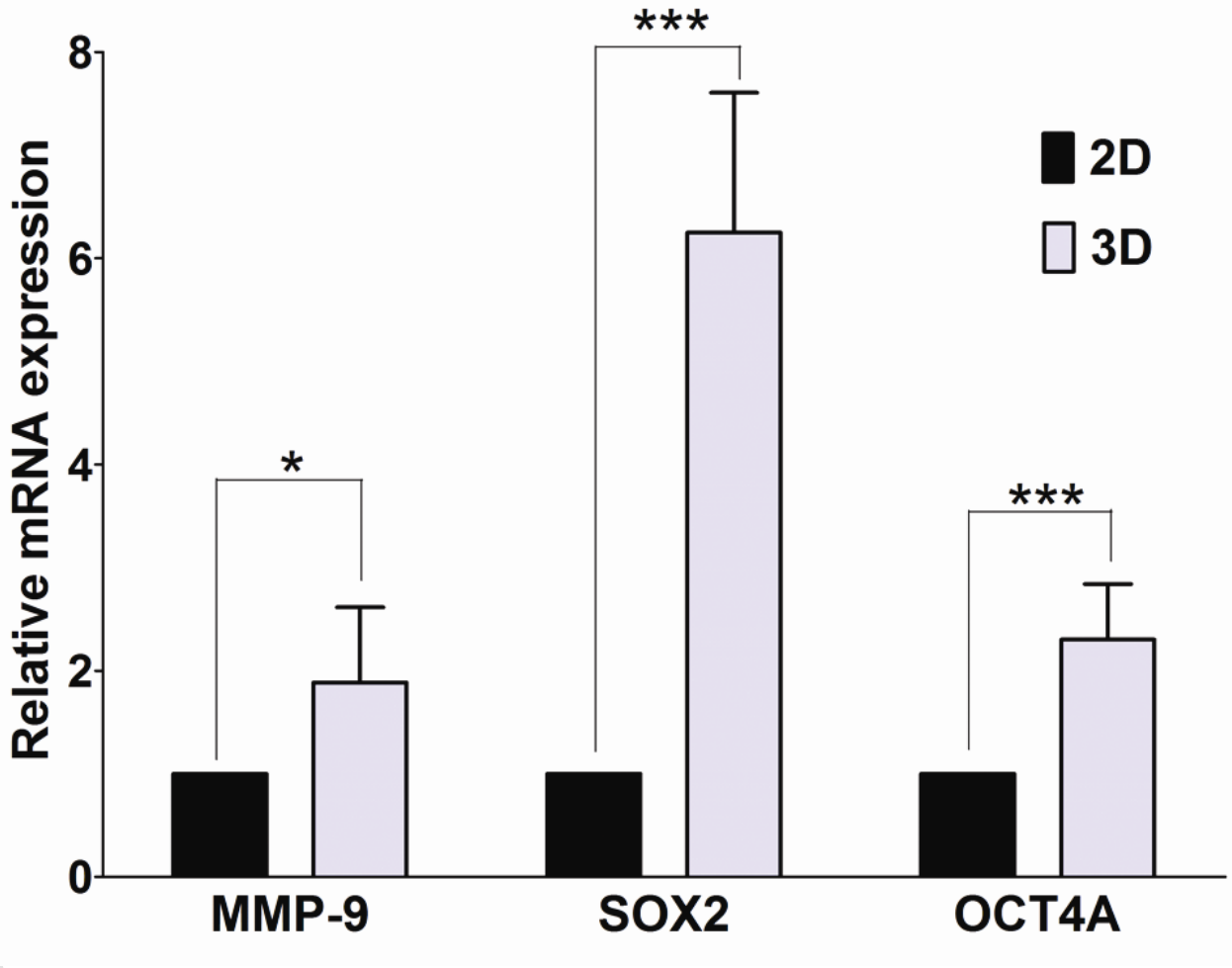

Figure 6

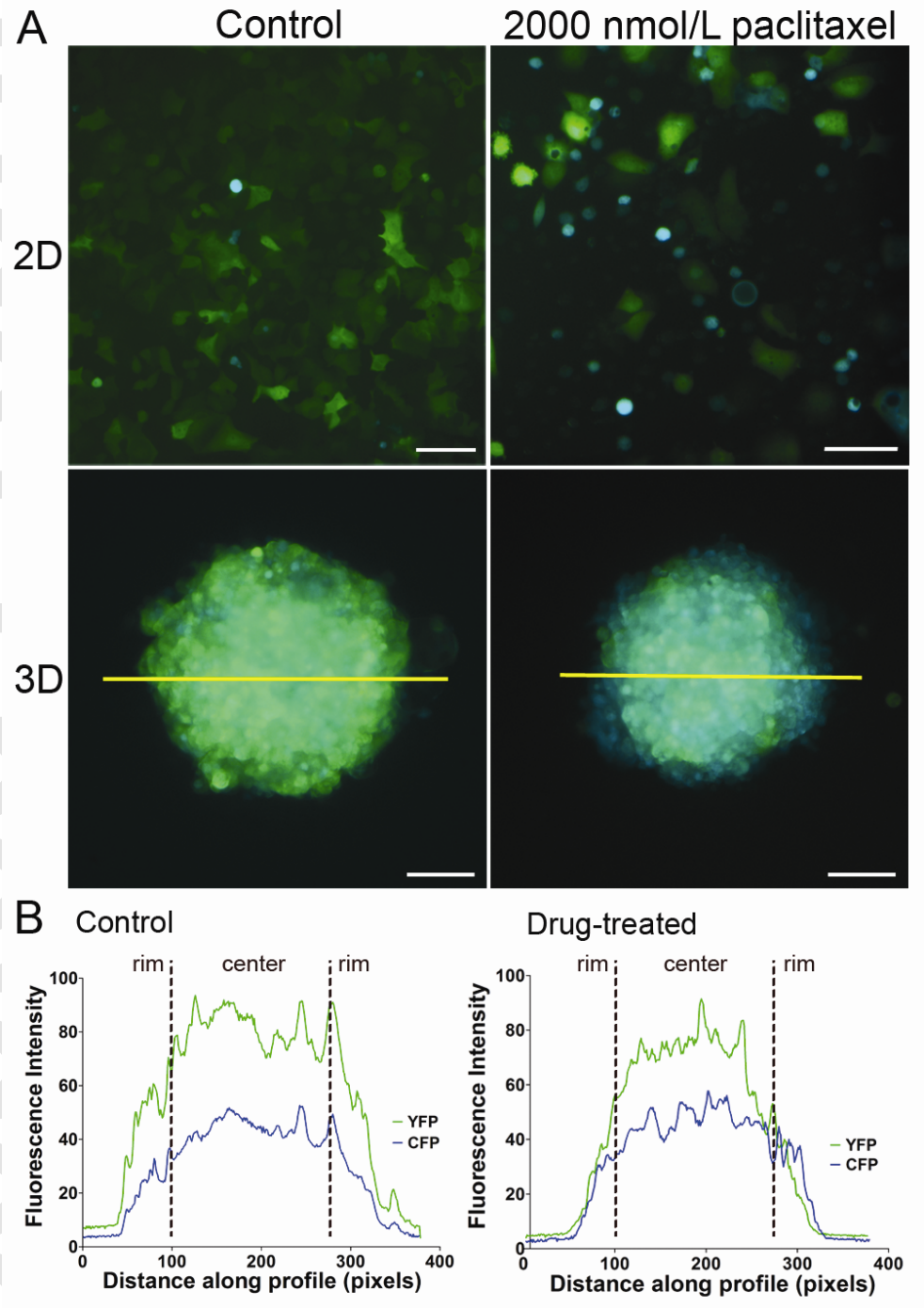

Figure 7